Electronic Conductivity, Ferrimagnetic Ordering, and Reductive Insertion Mediated by Organic Mixed-Valence in a Ferric Semiquinoid Metal–Organic Framework

Lucy E. Darago,[†] Michael L. Aubrey,[†] Chung Jui Yu,[†,#] Miguel I. Gonzalez,[†] and Jeffrey R. Long[*,†,‡,§]

[†]Department of Chemistry, University of California, Berkeley, California 94720, United States
[‡]Department of Chemical and Biomolecular Engineering, University of California, Berkeley, California 94720, United States
[§]Materials Sciences Division, Lawrence Berkeley National Laboratory, Berkeley, California 94720 United States

S Supporting Information

ABSTRACT: A three-dimensional network solid composed of Fe^{III} centers and paramagnetic semiquinoid linkers, $(NBu_4)_2$-$Fe^{III}_2(dhbq)_3$ ($dhbq^{2-/3-}$ = 2,5-dioxidobenzoquinone/1,2-dioxido-4,5-semiquinone), is shown to exhibit a conductivity of 0.16 ± 0.01 S/cm at 298 K, one of the highest values yet observed for a metal–organic framework (MOF). The origin of this electronic conductivity is determined to be ligand mixed-valency, which is characterized using a suite of spectroscopic techniques, slow-scan cyclic voltammetry, and variable-temperature conductivity and magnetic susceptibility measurements. Importantly, UV–vis–NIR diffuse reflectance measurements reveal the first observation of Robin–Day Class II/III mixed valency in a MOF. Pursuit of stoichiometric control over the ligand redox states resulted in synthesis of the reduced framework material $Na_{0.9}(NBu_4)_{1.8}Fe^{III}_2(dhbq)_3$. Differences in electronic conductivity and magnetic ordering temperature between the two compounds are investigated and correlated to the relative ratio of the two different ligand redox states. Overall, the transition metal–semiquinoid system is established as a particularly promising scaffold for achieving tunable long-range electronic communication in MOFs.
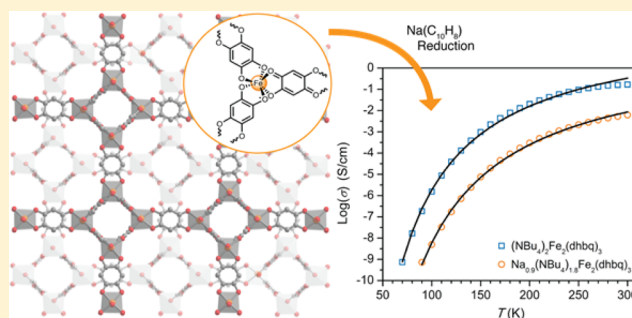
INTRODUCTION

Long-range electronic communication and its consequent properties, including charge mobility and, if unpaired spins are present, magnetic coupling, are highly dependent on the distances between the participating atoms or ions within a material. As such, the realization of electronic conductivity and magnetic ordering in low-density materials presents an intriguing objective—one that is seemingly at odds with itself. Reticular chemistry has been used with remarkable success, to produce extremely low-density, porous materials by design.[1] The resulting metal–organic frameworks (MOFs) are three-dimensional microporous materials composed of inorganic nodes and organic linkers. To date, this highly modular class of materials has proven most promising for applications in gas storage, separations, chemical sensing, and catalysis.[2] In contrast, engendering long-range charge transport and high-temperature magnetic ordering in this class of materials remains relatively unexplored. Mastery of these features could result in new applications for MOFs as battery electrodes, thermoelectrics, electrochemical sensors, electrocatalysts, bulk magnets, and magnetoelectrics or multiferroics.[3,4] Recent advances in the field have taken advantage of methods such as $\pi-\pi$ stacking, one-dimensional chain motifs that promote short metal–metal distances, and donor–acceptor pairings to achieve electronic conductivity.[5] Moreover, study of two-dimensional frameworks exhibiting strong $\pi-d$ conjugation has led to the observation of record electronic conductivities.[6] However, despite these notable examples, the field of MOFs exhibiting non-insulating electronic structures presents an exciting and open research frontier.

While solid-state permanent magnets and most electronic conductors rely on band-type electronic structures constructed from itinerant electrons, most MOFs are essentially ionic solids with large band gaps and little to no long-range electronic communication.[7] That is, their chemistry is localized and molecular in nature. Pervasive use of large diamagnetic linkers and oxophilic metal ions is in large part to blame. Although this combination helps promote framework stability, rigidity, and permanent porosity, it propagates large metal–metal distances, cutting off essential electronic exchange between the transition metal centered frontier orbitals responsible for charge transport and magnetic coupling.

The most promising means of gaining control over electronic structure in MOFs is through the strategic manipulation of metal–ligand frontier orbital overlap and energy match.

Judicious choice of metal and ligand, as well as the use of post-synthetic ion insertion, should enable control over electronic band gaps, carrier densities, magnetic coupling strength, and magnetic ordering behavior. To achieve a MOF with strong multi-dimensional electronic communication via this means, the metal and ligand should be open shell, have frontier orbitals of similar potential, and exhibit maximal orbital overlap to promote charge delocalization. While the topic of intra-molecular electron exchange has long fascinated the molecular inorganic chemistry community, the bounty of metal−ligand combinations known to produce significant charge delocalization, with the exception of several variations on the valence-ambiguous nickel−dithiolene system,[6c−f] has not yet been exploited in design of MOFs.

One of the best-known redox-active organic moieties with frontier orbitals energetically similar to those of the transition metals is 2,5-dihydroxybenzoquinone.[8] Three valence states of this ligand (Figure 1) are accessible in a variety of metal−organic motifs.[8a] Transition-metal-based systems containing the radical trianion $dhbq^{3-}$ reveal features characteristic of intramolecular charge delocalization, such as intervalence charge-transfer bands in their electronic absorption spectra and strong magnetic coupling.[9] Herein, we report a MOF constructed of Fe^{III} and mixed-valent $dhbq^{2-/3-}$ ligands that presents one of the highest conductivities yet observed for a MOF in addition to high-temperature magnetic interactions. We further demonstrate that this behavior is associated with the first instance of a Robin−Day Class II/III mixed-valency yet reported for a MOF. Finally, rare and precise control of reductive insertion within the porous structure is demonstrated to afford significant differences in electronic conductivity and magnetic ordering.

EXPERIMENTAL SECTION

General Information. All manipulations of $(NBu_4)_2Fe^{III}_2(dhbq)_3$ (**1**) following its initial synthesis were performed inside a N_2-filled glovebag or within the Ar atmosphere of a VAC Atmospheres glovebox. All reactions and subsequent manipulations for $Na_{0.9}$-$(NBu_4)_{1.8}Fe^{III}_2(dhbq)_3$ (**2**) were performed within the Ar atmosphere of a VAC Atmospheres glovebox. Tetrahydrofuran (THF) was dried using a commercial solvent purification system designed by JC Meyer Solvent Systems and subsequently stored over 4 Å molecular sieves. The compound 2,5-diaminobenzoquinone was prepared from 2,5-diaminohydroquinone dihydrochloride following a published procedure.[10] The compound 2,5-diaminohydroquinone dihydrochloride (97%) was purchased from Alfa Aesar and used as received. The compounds $Fe(SO_4)\cdot 7H_2O$ (≥99%) and tetrabutylammonium bromide (≥98%) were purchased from Sigma-Aldrich and used as received. All other chemicals were purchased from commercial vendors and used as received. Carbon, hydrogen, and nitrogen analyses were obtained from the Microanalytical Laboratory at the University of California, Berkeley.
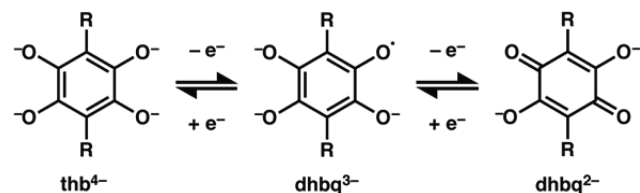
Figure 1. Redox states of linkers deriving from 2,5-dihydroxybenzo-quinone that have previously been observed in metal−organic molecules or coordination solids. Notably, $dhbq^{3-}$ is a paramagnetic radical bridging ligand.

**Synthesis of $(NBu_4)_2Fe^{III}_2(dhbq)_3$ (1).** A suspension of 20.0 mg (0.144 mmol) of 2,5-diaminobenzoquinone, 121 mg of $Fe(SO_4)\cdot 7H_2O$ (0.434 mmol), and 250 mg of tetrabutylammonium bromide (0.775 mmol) in 3.0 mL of deionized water titrated to a pH of 3.0 with concentrated HCl was loaded into a thick-walled borosilicate tube. The reaction suspension was degassed via four freeze−pump−thaw cycles, following which the tube was flame-sealed and loaded into an oven set to 120 °C. *Caution: improperly flame-sealed glass vessels may burst if heated above the boiling point of the reaction solvents they contain.* The suspension was heated at 120 °C for 24 h, at which point the tube was removed from the oven and allowed to cool to room temperature. After cooling, the resulting black cubic crystals were recovered via vacuum filtration inside a N_2-atmosphere glovebag. The product was dried by heating the solid crystals at 150 °C under reduced pressure for 1 h. Yield: 21.0 mg, 43%. Anal. Calcd for $C_{50}H_{78}Fe_2N_2O_{12}$: C, 59.41; H, 7.78; N, 2.77. Found: C, 59.19; H, 7.87; N, 2.93. IR (solid-ATR): 2956 (w), 2929 (w), 2869 (w), 2731 (w), 2538 (w), 1804 (w), 1488 (s), 1470 (s), 1364 (s), 1291 (m), 1270 (m), 1244 (s), 1208 (s), 1025 (m), 884 (m), 860 (s), 830 (m), 807 (s), 758 (m), 731 (m).

Synthesis of $Na_{0.9}(NBu_4)_{1.8}Fe^{III}_2(dhbq)_3$ (2). Prior to chemical reduction, cubic crystals of **1** were ground into a microcrystalline powder using a mortar and pestle in an Ar-atmosphere glovebox. Then, a stirred suspension of 50 mg (0.049 mmol) of **1** in 3.0 mL of THF was prepared. Na-naphthalenide was prepared by stirring 6.3 mg (0.049 mmol) of naphthalene ($C_{10}H_8$) over a roughly 10-fold excess of sodium metal in 2.0 mL of THF for 3 h. The resulting solution was filtered and added dropwise to the stirred suspension of **1** in THF at room temperature. The mixture was stirred for 12 h, after which **2** was recovered as a brown microcrystalline powder by vacuum filtration, washed with 2 × 2.0 mL of THF, and dried for 1 h under reduced pressure. Inductively coupled plasma (ICP) analysis indicated that 0.9 mol equiv of Na^+ ions was introduced per mole of **1**. Low percentages of C and H in elemental analysis indicated that roughly 10% of $(NBu_4)^+$ ions had been exchanged for Na^+. Thus, the true level of reduction in **2**, or otherwise stated the number of electrons introduced into framework **1**, was 0.7 e^- per mole of **1**. Two independently synthesized batches of **2** yielded identical elemental and ICP analyses. Yield: 46.0 mg, 96%. Anal. Calcd for $C_{46.8}H_{70.8}Fe_2N_{1.8}Na_{0.9}O_{12}$: C, 57.18; H, 7.26; N, 2.56. Found: C, 56.91; H, 7.07; N, 3.02. ICP Found: Fe:Na, 2.23(1):1. IR (solid-ATR): 2957 (w), 2931 (w), 2870 (w), 2738 (w), 2545 (w), 1820 (w), 1489 (s), 1470 (s), 1372 (s), 1292 (m), 1270 (m), 1246 (s), 1208 (s), 1026 (m), 876 (m), 861 (s), 830 (m), 807 (s), 758 (m), 731 (m).

RESULTS AND DISCUSSION

Synthesis and Characterization of $(NBu_4)_2Fe^{III}_2(dhbq)_3$ (1). Synthesis of **1** was performed under anaerobic conditions using the ligand 2,5-diaminobenzoquinone, which undergoes *in situ* hydrolysis to become $dhbq^{2-}$. The reaction of 3 mol equiv of $Fe(SO_4)\cdot 7H_2O$ with 1 equiv of 2,5-diaminobenzoquinone and excess tetrabutylammonium bromide in deoxygenated water for, titrated to a pH of 3.0, 24 h at 120 °C afforded **1** as black cubic crystals. Attempts to synthesize **1** starting with H_2dhbq rather than 2,5-diaminobenzoquinone only produced amorphous brown or black solids. The monohydrate of **1**, with the oxidation state assignment $(NBu_4)_2[Fe^{II}_2(dhbq^{2-})_3]\cdot H_2O$, was previously reported in ref 11. However, in our hands, some modification on this reported synthesis was required in order to obtain phase-pure **1**. Notably, if **1** was prepared under pH-neutral conditions, an unidentified ferromagnetic impurity, likely some form of Fe_2O_3, was co-precipitated with **1**, preventing an unqualified magnetic analysis.

The structure of **1** was elucidated using single-crystal X-ray analysis. The compound crystallizes in the cubic space group $I\bar{4}3d$ as two interpenetrated (10,3)-*a* nets of opposing chiralities (Figure 2d). In this topology, which is rare for $dhbq^{2-}$-based coordination solids,[11,12] neighboring metal centers within each
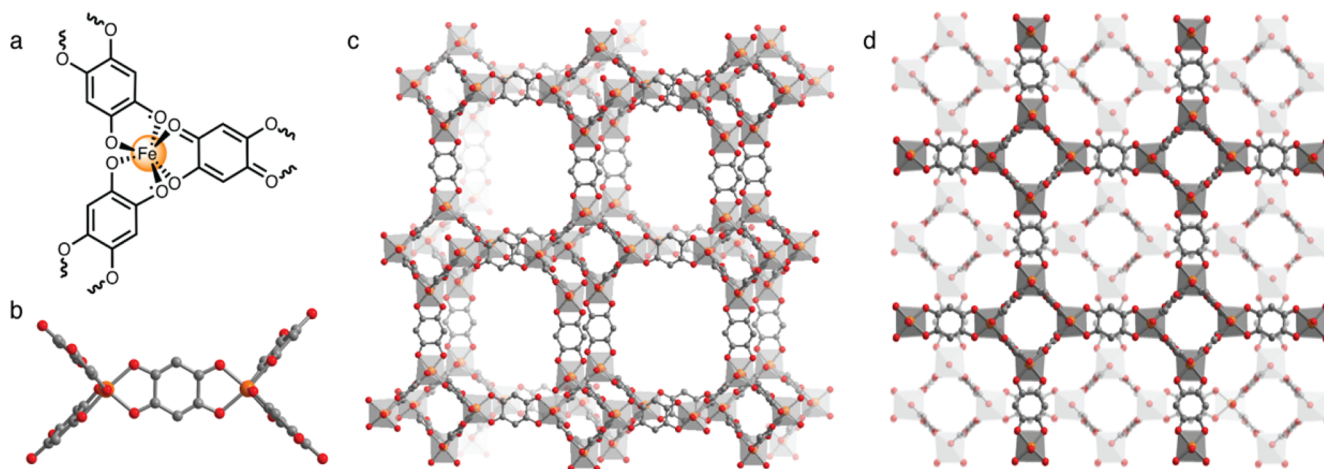
Figure 2. (a) Illustration of a single Fe^{III} center in **1**, showing that two radical ($dhbq^{3-}$) bridging ligands and one diamagnetic ($dhbq^{2-}$) bridging ligand are coordinated to each metal site. (b) A portion of the crystal structure of **1**, illustrating the local environment of two $dhbq^{n-}$-bridged Fe^{III} centers. (c) A larger portion of the crystal structure of **1**, showing one of the two interpenetrated (10,3)-*a* nets that together generate the porous three-dimensional structure. (d) The two interpenetrated (10,3)-*a* lattices of opposing chiralities that together compose **1**. Charge-balancing NBu_4^+ cations are not depicted for clarity.

lattice of **1** are all of the same chirality (Figure 2b,c), generating a three-dimensional structure. This differs from the classic two-dimensional honeycomb structure type frequently observed for coordination solids of $dhbq^{2-}$ and derivative ligands, in which neighboring metal centers are of opposing chiralities.[13] The tetrabutylammonium countercations in **1** were located crystallographically inside the pores and appear to be filling the pores near completely, with no large voids present. Interestingly, preliminary attempts at forming materials with the topology of **1** with smaller countercations, such as tetrapropylammonium or methyltributylammonium, have thus far proven unsuccessful. This may imply that the tetrabutylammonium cations are crucial to templating the three-dimensional structure of **1**, as transition metal coordination solids containing the $dhbq^{2-}$ ligand typically adopt one- or two-dimensional structures.[8a,13,14] Similar cation-dependent morphology changes have been observed for transition metal−oxalate coordination solids with the analogous chemical formula $[A^+]_2M^{II}_2(ox)_3$.[15] Two adsorption isotherms, 77 K N_2 and 195 K CO_2, were performed for **1** after heating at 150 °C under vacuum for 1 h, with both measurements confirming a lack of microporosity (Figure S1).

While an early indication of the intervalence charge transfer present in **1** came from its black color, as coordination solids composed solely of the dianionic $dhbq^{2-}$ ligand are typically bright or dark red,[8a,10] the crystal structure analysis provided additional evidence that electron transfer had taken place during synthesis (Table S1 and Figure S2). The Fe−O distances in **1** are 2.008(7) and 2.031(7) Å, significantly shorter than the Fe−O distances in Fe^{II}-based molecules and coordination solids containing dhbq-type ligands.[8a,9,16] Additionally, C−O distances for the $dhbq^{n-}$ ligands in **1** are slightly longer (1.281(11) and 1.308(12) Å) than those observed for $dhbq^{2-}$ coordination complexes (typically in the 1.26−1.29 Å range).[8a]

Mössbauer spectroscopy was used to unequivocally establish the oxidation state of the iron centers in **1**. At 100 K, the ^{57}Fe Mössbauer spectrum (Figure 3) is comprised of a doublet with an isomer shift of $\delta = 0.574(2)$ mm/s, a quadrupole splitting of $|\Delta E_Q| = 1.279(5)$ mm/s, and a line width of $\Gamma = 0.326(8)$ mm/s (Figure 3, top). These parameters are similar to those of other

high-spin Fe^{III} compounds; the isomer shift, in particular, is quite close to those exhibited by mononuclear high-spin Fe^{III} molecules ligated by three semiquinones.[17] The large quadrupole splitting is consistent with the extensive π-bonding presumed to occur in the compound. The Mössbauer spectrum does not show any significant changes across the temperature range 20−300 K. Below 20 K, however, a poorly resolved sextet begins to appear as a consequence of magnetic ordering in **1**.

The observations made from crystallographic analysis and Mössbauer spectroscopy led to the assignment of **1** as $(NBu_4)_2Fe^{III}_2(dhbq)_3$. Concomitant with the assignment of the iron centers as trivalent is the assumption that at least some of the $dhbq^{n-}$ ligands are spontaneously reduced by Fe^{II} during the synthesis in order to generate a charge-balanced material. Separate one-electron redox couples for $dhbq^{2-}/dhbq^{3-}$ and $dhbq^{3-}/thb^{4-}$ have been observed in previous work on $dhbq^{2-}$-containing molecules.[9] Thus, the ligands in **1** were assumed to be a combination of the $dhbq^{2-}$ and the organic radical $dhbq^{3-}$ oxidation states. Ignoring the possibility of ligand-based redox non-innocence, in order to achieve charge balance, the ligand redox states should be a 2:1 ratio of $dhbq^{3-}$ to $dhbq^{2-}$ (Figure 2a).

Slow-Scan Cyclic Voltammetry. In order to better understand the redox behavior of **1**, slow-scan cyclic voltammetry (SSCV) was performed. This technique, while in common use for inorganic intercalation solids, has passed largely unutilized for redox-active MOFs. This may be the result of the assumption that most MOFs are completely insulating, prompting the use of fast-scanning CV techniques that only investigate redox activity at the crystallite surface. However, a number of recent reports have addressed the reductive insertion of lithium ions in certain MOFs using galvanostatic methods.[18]

A voltammogram of **1** using lithium reference and counter electrodes in 0.1 M $LiBF_4$ in propylene carbonate was collected at a scan rate of 30 μV/s (Figure 4). Given a tentative composition of $Li_x[NBu_4]_2Fe^{III}_2(dhbq)_3$, the material could be reduced to $x = 3.7$ quasi-reversibly with 77% Faradaic efficiency. Despite this relatively low Faradaic efficiency for a reductive insertion reaction, we were encouraged by the possibility of reducing **1** to a composition with a radical located on every
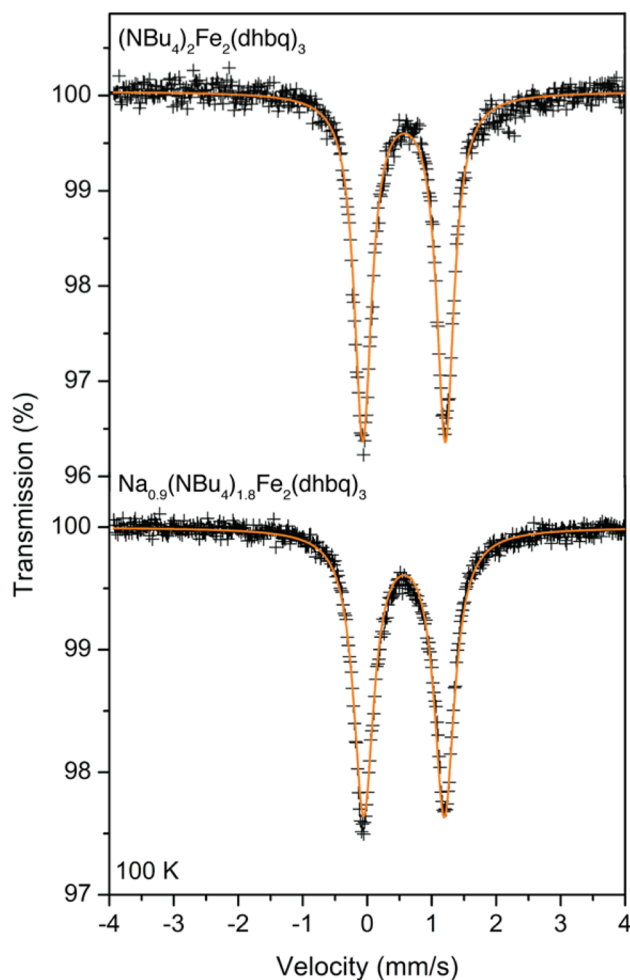
Figure 3. ^{57}Fe Mössbauer spectra for **1** (top) and **2** (bottom) at 100 K, with the fits to the spectra shown in orange. Both fits have parameters consistent with high-spin Fe^{III}.

ligand in the framework. Integration of the first quasi-reversible peak corresponds to 1.1 electrons per mole of **1**. This one-electron couple likely corresponds to reduction of the remaining dhbq^{2-} ligand in **1** to a dhbq^{3-} radical. Moreover, the total reduction activity observed, close to 4 e$^-$ per mole of **1**, is postulated to correspond to solely ligand-based reduction activity, since a four-electron reduction would correspond to reduction of all three dhbq^{n-} ligands to the thb^{4-} oxidation state. As discussed below, these expectations are consistent with chemical reduction reactions using sodium naphthalenide as a stoichiometric reductant, as probed via Mössbauer spectroscopy of the resulting products. In light of the results from the chemical reductions, we expected the Fe$^{II/III}$ redox manifold to be accessible at more reducing potentials. Unfortunately, attempts to electrochemically reduce the material beyond $x = 3.7$ resulted in decomposition of the framework.

Chemical Reduction of 1. A one-electron chemical reduction of **1** was pursued using a stoichiometric amount of sodium naphthalenide in THF. The recovered product was studied using ICP analysis and discovered to have a Fe:Na ratio of 2.23(1):1. In addition, elemental analysis revealed low amounts of carbon and hydrogen, indicating a small exchange (10%) of NBu$_4^+$ cations for Na$^+$. The combination of these analyses supports an assignment of the formula unit of the reduced material as Na$_{0.9}$(NBu$_4$)$_{1.8}$Fe$_2$(dhbq)$_3$ (**2**), which

corresponds to a 0.7 e$^-$/mol reduction of **1**. The reduced framework shows a highly crystalline powder X-ray diffraction (PXRD) pattern that almost perfectly overlays with that simulated for **1**, indicating little if any change in unit cell (Figure S3).

The Mössbauer spectrum of **2** (Figure 3, bottom) also shows little change compared to that of **1**, indicating that the ligands, not the Fe^{III} centers, were reduced during the chemical reduction. Compound **2** exhibits an isomer shift of $\delta = 0.570(3)$ mm/s, a quadrupole splitting of $|\Delta E_Q| = 1.252(7)$ mm/s, and a line width of $\Gamma = 0.381(6)$ mm/s, parameters that are very similar to those observed for **1**. Again ignoring possible ligand-based redox non-innocence, in order to achieve a charge balanced material the ligand redox states in **2** should be a 2.7:0.3 ratio of dhbq^{3-} to dhbq^{2-}. Notably, the iron sites in this material are close to fully bridged by the radical trianion linker dhbq^{3-}.

A further chemical reduction was performed using 4 equiv of sodium naphthalenide per mole of **1** (see the Supporting Information) in order to determine whether the redox chemistry observed in the electrochemical analysis was entirely ligand-based, or partially metal-based. ICP analysis indicated that the resulting product has a putative chemical formula of Na$_{3.2}$(NBu$_4$)$_{1.8}$Fe$_2$(dhbq)$_3$. As with **2**, the resulting PXRD pattern almost perfectly overlays with that of **1** (Figure S4). Mössbauer spectroscopy at 100 K revealed two iron sites (Figure S5). The first site, accounting for 51% of the iron centers, exhibits $\delta = 0.47(3)$ mm/s, $|\Delta E_Q| = 0.79(2)$ mm/s, and $\Gamma = 0.50(5)$ mm/s, while the second site, corresponding to 49% of the iron centers, exhibits $\delta = 0.58(1)$ mm/s and $|\Delta E_Q| = 1.26(3)$ mm/s, and $\Gamma = 0.36(2)$ mm/s. Since both sites have parameters consistent with Fe^{III}, chemical reduction of **1**—at least up to 3 equiv of Na$^+$ per mole—appears to be ligand-based, generating first dhbq^{3-} and then thb^{4-} ligands. On the basis of its hyperfine parameters, the first site could possibly be assigned to low-spin Fe^{II}, but at this time, the assignment to high-spin Fe^{III} is preferred. This further chemical reduction of **1**, and other chemical reductions beyond 0.7 e$^-$/mol of **1**, are still under investigation due to the presence of multiple iron
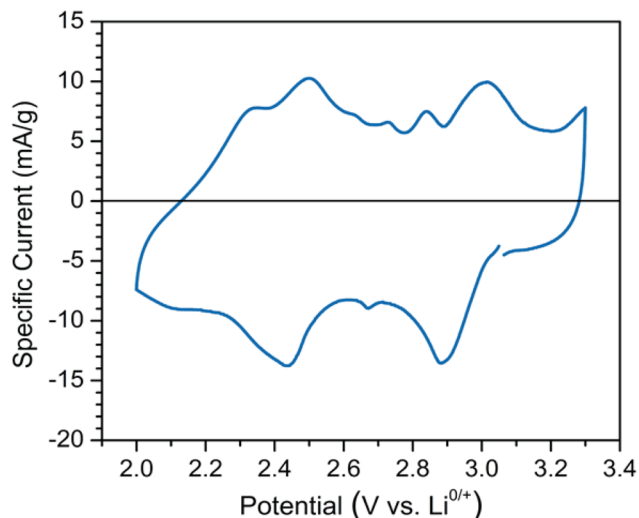
Figure 4. Slow-scan cyclic voltammetry of **1**. Lithium reference and counter electrodes were used with an electrolyte solution of 0.1 M LiBF$_4$ in propylene carbonate. A scan rate of 30 μV/s was used. The data shown use the IUPAC current convention.
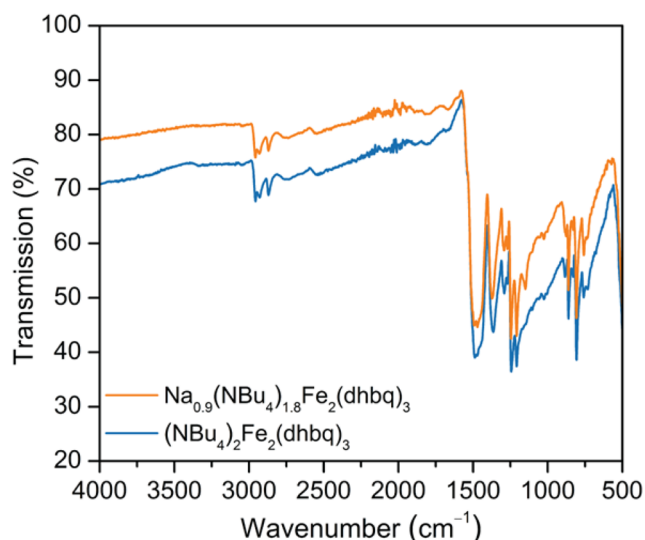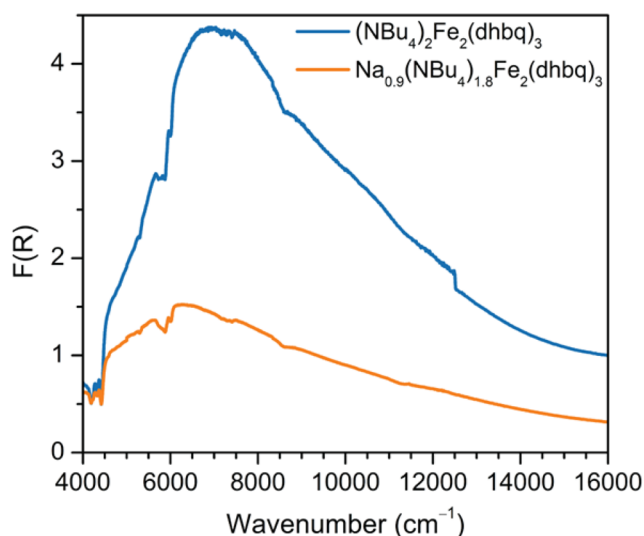
Figure 5. Infrared spectra of **1** and **2** shown in blue and orange, respectively.

Figure 6. Diffuse reflectance UV−vis−NIR spectra of **1** and **2** shown in blue and orange, respectively. $F(R)$ is a Kubelka−Munk conversion of the raw diffuse reflectance spectrum.

sites lending additional complexity to their electronic structures. Thus, only frameworks **1** and **2** will be discussed further here.

Infrared Spectroscopy. With the valency of the iron cations in **1** and **2** established, the valence of the ligands was further studied using IR spectroscopy. The spectrum of **1** (Figure 5) presents broad mid-IR absorption suggestive of intervalence charge transfer. In addition, the high degree of asymmetry of the peaks in the spectra for **1** and **2** is likely due to significant coupling of electronic modes to vibronic modes, a feature also associated with intervalence charge transfer (IVCT). Crucially, both spectra display a very broad peak over $1510-1450$ cm^{-1}, which we assign to the C=O stretching vibration. This stretch is typically much sharper and at higher wavenumbers for materials containing only the $dhbq^{2-}$ ligand.[8a] Moreover, in $dhbq^{2-}$-containing molecules, this stretch is typically observed to shift to lower energy by ~50 cm^{-1} when reduced to $dhbq^{3-}$.[9] Thus, the appearance of one broad stretch or possibly two overlapping stretches across the $1510-1450$ cm^{-1} region supports assignment of the $dhbq^{n-}$ ligands as $dhbq^{2-/3-}$. This broad C=O stretch, in addition to the broad absorbance in the mid-IR region, encouraged further investigation of ligand intervalence using UV−vis−NIR spectroscopy.

UV−Vis−NIR Diffuse Reflectance Spectroscopy. The electronic absorption spectra of **1** and **2** (Figure 6) show a broad absorbance extending across the range $4500-14\,000$ cm^{-1}, with ν_{max} = 7000 and 6300 cm^{-1}, respectively. These intense absorption features are attributed to ligand-based IVCT. Notably, a solid-state UV−vis−NIR spectrum of a molecular Fe^{III} semiquinone−catecholate compound shows a similar, though narrower, IVCT band at ν_{max} = 5200 cm^{-1}.[19] Since all of the iron centers in **1** and **2** were confirmed to be trivalent by Mössbauer spectroscopy, the origin of the IVCT must be the organic $dhbq^{2-/3-}$ moieties. Interestingly, in both cases the bands display a very sharp absorption edge at low energy (4500 cm^{-1}), one of the best-known signatures of Robin−Day Class II/III mixed-valency.[20] This represents the first observation of a Class II/III mixed-valency in a MOF of which we are aware, and provides a definitive signature of strong electronic correlation within these materials. A higher

energy absorbance observed at 21 500 cm^{-1} is tentatively assigned to a $\pi-\pi^*$ transition, though the feature may also be due to ligand-to-metal charge transfer (Figure S6). The observation of a low-lying IVCT band in the electronic absorption spectra of **1** and **2** is indicative of thermally activated charge transport within the lattice, and this motivated us to explore the electronic conductivity of these materials.

MOFs seldom exhibit either metal[5d,18,21] or ligand[5c,f,6c,18,22] redox activity, and control of the redox states in a framework is even more rarely achieved. Post-synthetic chemical redox reactions of MOFs are typically performed using a large excess of a redox reagent or not quantified, making full characterization of the resulting products difficult. Also, the majority of ligand redox activity observed in MOFs thus far has been characterized using spectroelectrochemical measurements, in contrast to post-synthetic analysis of bulk redox reaction products. Thus, the synthesis of **1** and **2** provided a unique opportunity to study a pair of materials with precise chemical redox states and correlate their electronic and magnetic behaviors.

Electronic Conductivity. Electronic conductivity was investigated via two-point dc conductivity measurements performed on pressed pellets of **1** and **2**. For compound **1**, a room-temperature conductivity of 0.16(1) S/cm was determined and found to be Ohmic within ±1 V of open circuit. To the best of our knowledge, this is the highest conductivity value yet observed for a three-dimensionally connected MOF. While several higher values have been reported for lamellar solids, the mode of conductivity in these materials is often attributed to π−d conjugation through square planar metal centers.[6f] To date, no clear strategy of extending this mechanism to three-dimensional solids has emerged. In contrast, compound **2** was found to be considerably less conductive, exhibiting a conductivity of 0.0062(1) S/cm at 298 K.

The foregoing results suggest a mode of conductivity consistent with electron hopping within the $dhbq^{2-/3-}$ redox manifold. Considering the reduction to yield **2**, this model would agree that with population of the $dhbq^{2-}$ vacancies, such that fewer unpaired electrons on radical $dhbq^{3-}$ linkers have a nearest neighbor $dhbq^{2-}$ vacancy to hop to, the carrier mobility
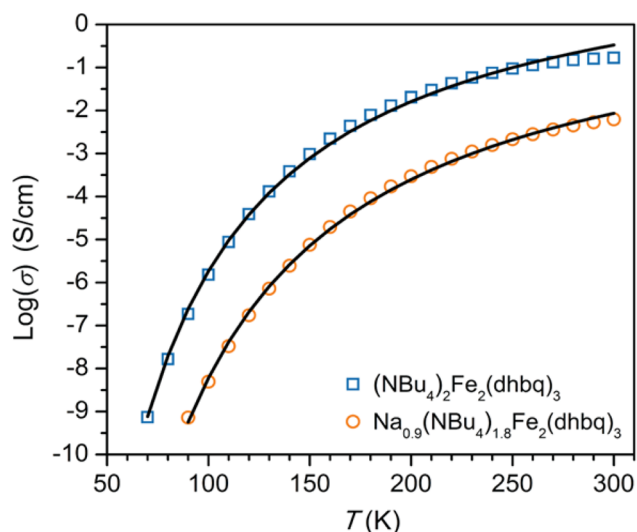
Figure 7. Variable-temperature conductivity data for **1** and **2**, shown by blue squares and orange circles, respectively. Arrhenius fits to the data are shown by black lines.

and in turn the conductivity should indeed decrease. As such, fractional oxidation of **1** could be expected to yield even higher conductivities. Unfortunately, clean synthetic conditions for the oxidative de-insertion of the tetrabutylammonium cations have not yet been identified.

Variable-temperature conductivity measurements were performed in the temperature range 70–300 K. Both **1** and **2** were confirmed to be semiconducting, with an Arrhenius temperature dependence. An Arrhenius fit to the data revealed an activation energy of just 110 meV for **1** (Figures 7, S7, and S8). In contrast, a considerably larger activation energy of 180 meV was obtained for **2** (Figures 7 and S7–S9). The stronger temperature dependence of the conductivity for **2** is again consistent with a further divergence of the $dhbq^{3-}:dhbq^{2-}$ ligand ratio from the optimal mixed-valence ratio of 1:1.

While it is expected that the conductivity results obtained by two-point pressed pellet measurements may be limited by crystallite boundaries and electrode contacts, the activation energies of **1** and **2** are of reasonable magnitude to be consistent with the broad, low-energy absorption bands observed in the IR and UV–vis–NIR spectra. The cubic symmetry of the conduction pathway is quite rare for conductive coordination solids. It was found to be advantageous in this case, however, owing to mitigation of the texturing effects often observed in pressed pellet measurements of one- and two-dimensional conductors. A final consideration is that while the carrier mobility should decrease as the stoichiometry moves further from that of optimal mixed-valence, the charge carrier density should increase as more $dhbq^{2-}$ ligands are reduced to radical $dhbq^{3-}$ species. Our present work suggests that charge carrier mobility is the greater predictor of conductivity in these materials, as **2** is less conductive than **1**.

Magnetic Properties. Concurrently, the presence of $dhbq^{3-}$ radicals in **1** and **2** prompted us to investigate their magnetic behaviors. Previously studied metal–organic materials with transition metals bridged by organic radicals have demonstrated strong magnetic coupling, leading to high-temperature magnetic ordering.[23] The most famous example is the room-temperature magnet $V(TCNE)_2 \cdot xCH_2Cl_2$ (TCNE = tetracyanoethylene).[24] Variable-temperature dc magnetic

susceptibility measurements of **1** under an applied magnetic field of 0.1 T revealed strong metal-radical magnetic interactions, eventually leading to magnetic ordering at 8 K (Figure 8, top). The ordering temperature, confirmed using ac magnetic susceptibility measurements (Figure S10), was significantly lower than anticipated based on the strong magnetic coupling that has previously been observed in Fe^{III}-$dhbq^{3-}$ molecules.[9c] However, strong deviations from Curie–Weiss behavior below 250 K shed some light onto the low magnetic ordering temperature (Figure 8, middle). Such deviations from Curie–Weiss behavior have been previously observed in systems with strong π–d interactions,[25] and have also been attributed to local magnetic order (in contrast to bulk magnetic ordering) or competing ferromagnetic and antiferromagnetic interactions leading to magnetic glassiness,[26] both of which could be present in **1**.

A Curie–Weiss fit of the inverse magnetic susceptibility data for **1** from 250 to 300 K results in a Curie temperature of $\theta = 134$ K and a Curie constant of $C = 6.1$ emu·K/mol. The positive Curie temperature reveals that ferromagnetic interactions are dominant at high temperature in **1**, and its magnitude suggests that quite high temperature magnetic coupling occurs in **1**. In contrast, the magnetic behavior at low temperature indicates that ferrimagnetic coupling predominates. The shape of the magnetization (Figure S11) versus temperature from 40 to 2 K is a gradual, nearly linear increase, rather than the sharp increase and magnetization saturation typically associated with bulk ferromagnets. In addition, low-temperature magnetic hysteresis data reveal a saturation magnetization of 7.3 μ_B/mol, much closer to the 8.94 μ_B/mol expected for ferrimagnetic coupling rather than the 10.95 μ_B/mol expected for ferromagnetic coupling. Thus, the low magnetic ordering temperature of **1** is attributed to a competition of ferromagnetic and antiferromagnetic interactions that prevents true three-dimensional order, until antiferromagnetic metal–radical interactions, and thus bulk ferrimagnetic order, prevail at low temperature.

Compound **2**, which is much closer to a fully $dhbq^{3-}$-bridged framework, was expected to show an increased magnetic ordering temperature due to the greater number of paramagnetic linkers. Indeed, a higher magnetic transition temperature of 12 K was observed, as determined using ac magnetic susceptibility measurements (Figure S10). The room-temperature product of magnetic susceptibility and temperature ($\chi_M T$) for **2** is 11.2 emu·K/mol, compared to 10.9 emu·K/mol for **1**. Accordingly, the difference between the two frameworks is 0.3 emu·K/mol at 300 K, close to the 0.26 emu·K/mol difference expected with addition of 0.7 equiv of an $S = 1/2$ spin, assuming magnetically isolated metal and radical spins. Moreover, Curie–Weiss analysis of the magnetic susceptibility data for **2** in the temperature range 250–300 K results in $\theta = 144$ K and $C = 5.90$ emu·K/mol (Figure 8, middle). The higher Curie temperature as compared to **1** is in keeping with the greater density of magnetic exchange interactions expected for **2**.

Finally, low temperature (2 K) magnetic hysteresis measurements reveal that **2** is a harder magnet than **1**, with coercive fields of 350 and 100 Oe observed, respectively (Figure 8, bottom). The saturation magnetization (Figure S12) of **2** is 7.11 μ_B/mol, lower than that of **1**, as expected due to the additional ligand radical spins coupling antiferromagnetically to the Fe^{III} centers, and close to the predicted value of 7.94 μ_B/mol for ferrimagnetic coupling. The lower than predicted
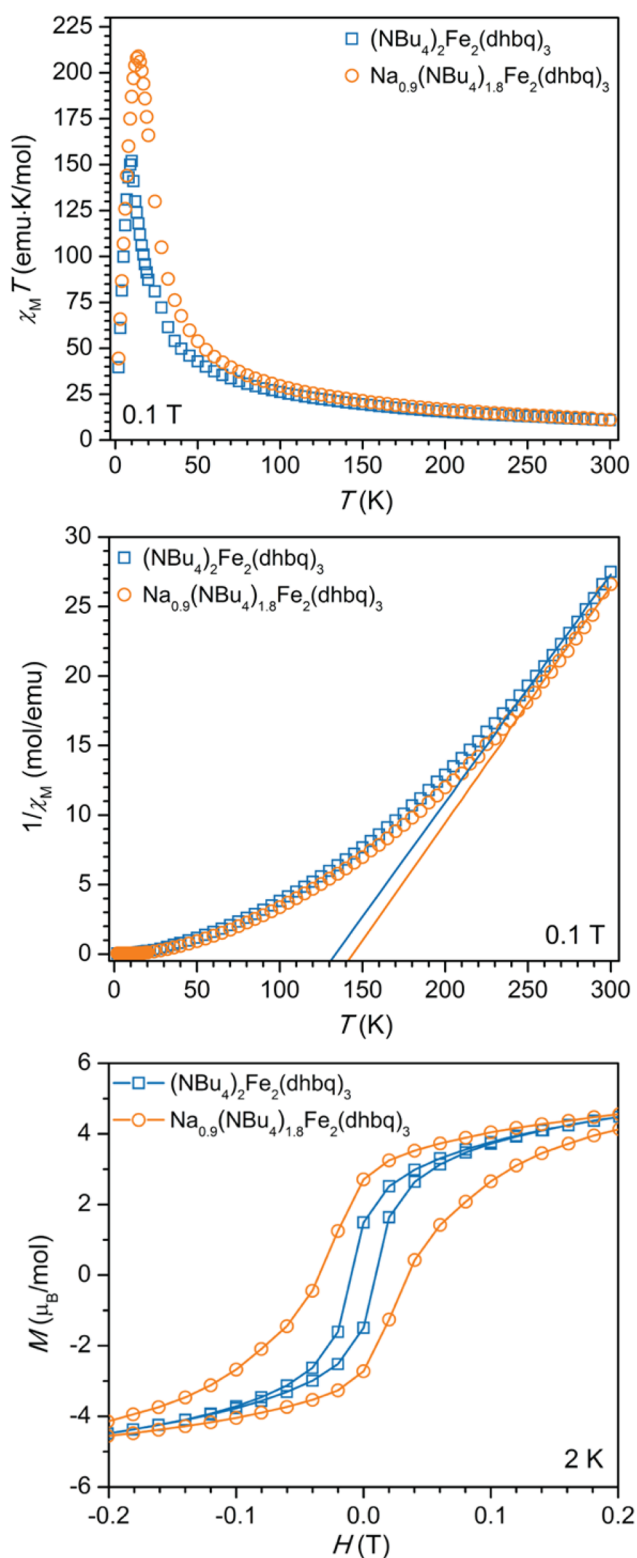
Figure 8. Top: Dc magnetic susceptibility data for **1** and **2** represented by blue squares and orange circles, respectively. Middle: Inverse of magnetic susceptibility versus temperature for **1** and **2**. Curie−Weiss fits to the data in the temperature range 250−300 K are shown by solid blue and orange lines for **1** and **2**, respectively. Bottom: Magnetization (*M*) versus applied dc magnetic field (*H*) data for **1** and **2** in blue and orange, respectively. Hysteresis loops were recorded at a sweep rate of 2 mT/s. Solid lines are guides for the eye. Figure S12 shows the full hysteresis loops in an applied dc magnetic field range of −7 to 7 T.

saturation magnetization values of both **1** and **2** at low temperature are attributed to antiferromagnetic interactions between the two sublattices that comprise the framework. In general, the conflict between the high Curie temperatures observed for **1** and **2** and their comparatively low magnetic ordering temperatures can potentially be resolved by counterion changes. Altering the counterion A^+ in the two-dimensional materials $[A^+]Fe^{II}Fe^{III}(oxalate)_3$, for example, has been shown to shift their magnetic ordering temperatures across a temperature range of 17 K.[23,27]

Interestingly, the foregoing results qualitatively adhere to the relation between the number of magnetic neighbors (z) and magnetic ordering temperature, $T_C \propto z$, first introduced by Néel and later popularized during magnetic studies of Prussian blue analogues.[28] As a result, we believe there is an exciting future in chemically tuning metal−organic radical frameworks to maximize the number of magnetic neighbors and the magnitude of metal−radical magnetic coupling in order to achieve high-temperature magnetic ordering.

■ CONCLUSIONS AND OUTLOOK

Overall, the work herein extends the oft-praised tunability of metal−organic frameworks to affect electronic structure, enabling control over bulk electronic and magnetic properties. Ongoing efforts are directed toward altering the transition metal, linker substituents, and charge-balancing cations in **1** to control the mixed-valency behavior, provoking changes in magnetic ordering temperature and electronic conductivity. In addition, we believe that further work on the transition metal−semiquinoid framework studied here could potentially expose new applications for MOFs. For instance, organic mixed-valence has long been considered an appealing means for achieving high gravimetric density electrochemical energy storage, despite the common pitfall of large structural changes upon reduction or oxidation that result in limited cyclability.[29] MOFs with redox-active linkers can circumvent this issue since the redox-active moieties are locked within a rigid metal−ligand lattice. While the materials studied here show only quasi-reversible ligand redox couples, ion exchange of the tetrabutylammonium ions for smaller cations may engender permanent porosity in **1**, allowing for ion-insertion with enhanced reversibility. Further, chemical oxidation of **1** to the charge neutral $Fe^{III}_2(dhbq^{2-})_3$ formula could result in a framework whose pores are filled only by solvent. This hypothetical material is predicted[30,31] to have a large accessible surface area of 5070 m^2/g upon activation and could likely support both cation and anion insertion. Overall, the $Fe_2(dhbq)_3$ system could potentially exhibit up to 8 electrons per formula unit of redox activity, making it an intriguing candidate for MOF-based electrodes.

Furthermore, magnetic ordering and semiconducting or metallic behaviors typically stem from separate sub-lattices when observed in the same coordination solid, such as in tetrathiafulvalene salts with paramagnetic counterions.[32] In contrast, materials like **1** and **2**, for which the electronic and magnetic properties extend from the same origin (in this case the ferric semiquinoid lattice), present an especially valuable opportunity to pursue magnetoelectric or multiferroic MOFs.

In conclusion, the foregoing work demonstrates a rare example of a MOF composed of metal ions bridged by paramagnetic linkers that additionally displays ligand mixed-valency. The effects of ligand-mixed valency on the electronic, magnetic, and ion-insertion behaviors of the framework have

been explored. Importantly, the electronic conductivities obtained are some of the highest yet observed for MOFs, indicating that ligand mixed-valency can serve as a highly effective charge transport mechanism within MOFs. Also included is one of the first instances of post-synthetic chemical redox control over a MOF. Specifically, control over the ligand redox states in the framework was established using post-synthetic chemical redox reactions, resulting in synthesis of a 0.7-electron reduction of framework **1**. Correlated changes in electronic conductivity and magnetic ordering temperature were observed for the two frameworks. Explicitly, this work establishes the transition metal—semiquinoid system as a promising scaffold for delocalized and tunable electronic structures in MOFs. More broadly, it highlights the technique of post-synthetic redox control over a MOF as a means to achieving specific desired electronic properties, enabling new applications for these materials in electronic devices.

■ ASSOCIATED CONTENT

Ⓢ Supporting Information

The Supporting Information is available free of charge on the ACS Publications website at DOI: 10.1021/jacs.5b10385.

> Additional experimental procedures and PXRD, Mössbauer spectroscopy, UV–vis–NIR diffuse reflectance, variable-temperature conductivity, and variable-temperature magnetism data (PDF)
> Crystallographic data for **1** (CIF)

■ AUTHOR INFORMATION

Corresponding Author
*jrlong@berkeley.edu

Present Address
#C.J.Y.: Department of Chemistry, Northwestern University, Evanston, IL 60208, USA

Notes
The authors declare no competing financial interest.

■ ACKNOWLEDGMENTS

■ REFERENCES

(1) (a) Furukawa, H.; Go, Y. B.; Ko, N.; Park, Y. K.; Uribe-Romo, F. J.; Kim, J.; O'Keeffe, M.; Yaghi, O. M. *Inorg. Chem.* **2011**, *50*, 9147. (b) Farha, O. K.; Eryazici, I.; Jeong, N. C.; Hauser, B. G.; Wilmer, C. E.; Sarjeant, A. A.; Snurr, R. Q.; Nguyen, S. T.; Yazaydın, A. Ö.; Hupp, J. T. *J. Am. Chem. Soc.* **2012**, *134*, 15016. (c) Furukawa, H.; Cordova, K. E.; O'Keeffe, M.; Yaghi, O. M. *Science* **2013**, *341*, 1230444.

(2) (a) Eddaoudi, M.; Kim, J.; Rosi, N.; Vodak, D.; Wachter, J.; O'Keeffe, M.; Yaghi, O. M. *Science* **2002**, *295*, 469. (b) Kreno, L. E.; Leong, K.; Farha, O. K.; Allendorf, M.; Van Duyne, R. P.; Hupp, J. T. *Chem. Rev.* **2012**, *112*, 1105. (c) Sumida, K.; Rogow, D. L.; Mason, J. A.; McDonald, T. M.; Bloch, E. D.; Herm, Z. R.; Bae, T.-H.; Long, J. R. *Chem. Rev.* **2012**, *112*, 724. (d) Zhou, H.-C. J.; Kitagawa, S. *Chem. Soc. Rev.* **2014**, *43*, 5415. (e) Corma, A.; García, H.; Llabrés i Xamena, F. X. *Chem. Rev.* **2010**, *110*, 4606.

(3) Electronics applications: (a) D'Alessandro, D. M.; Kanga, J.; Caddy, J. S. *Aust. J. Chem.* **2013**, *64*, 718. (b) Morozan, A.; Jaouen, F. *Energy Environ. Sci.* **2012**, *5*, 9269. (c) Erickson, K. J.; Léonard, F.; Stavila, V.; Foster, M. E.; Spataru, C. D.; Jones, R. E.; Foley, B. M.; Hopkins, P. E.; Allendorf, M. D.; Talin, A. A. *Adv. Mater.* **2015**, *27*, 3453.

(4) Magnetism applications: (a) Kurmoo, M. *Chem. Soc. Rev.* **2009**, *38*, 1353. (b) Dechambenoit, P.; Long, J. R. *Chem. Soc. Rev.* **2011**, *40*, 3249. (c) Coronado, E.; Mínguez Espallargas, G. *Chem. Soc. Rev.* **2013**, *42*, 1525.

(5) (a) Givaja, G.; Amo-Ochoa, P.; Gómez-García, C. J.; Zamora, F. *Chem. Soc. Rev.* **2012**, *41*, 115. (b) Takaishi, S.; Hosoda, M.; Kajiwara, T.; Miyasaka, H.; Yamashita, M.; Nakanishi, Y.; Kitagawa, Y.; Yamaguchi, K.; Kobayashi, A.; Kitagawa, H. *Inorg. Chem.* **2009**, *48*, 9048. (c) Kobayashi, Y.; Jacobs, B.; Allendorf, M. D.; Long, J. R. *Chem. Mater.* **2010**, *22*, 4120. (d) Gándara, F.; Uribe-Romo, F. J.; Britt, D. K.; Furukawa, H.; Lei, L.; Cheng, R.; Duan, X.; O'Keeffe, M.; Yaghi, O. M. *Chem. - Eur. J.* **2012**, *18*, 10595. (e) Narayan, T. C.; Miyakai, T.; Seki, S.; Dincă, M. *J. Am. Chem. Soc.* **2012**, *134*, 12932. (f) Sun, L.; Miyakai, T.; Seki, S.; Dincă, M. *J. Am. Chem. Soc.* **2013**, *135*, 8185. (g) Talin, A. A.; Centrone, A.; Ford, A. C.; Foster, M. E.; Stavila, V.; Haney, P.; Kinney, R. A.; Szalai, V.; El Gabaly, F.; Yoon, H. P.; Léonard, F.; Allendorf, M. D. *Science* **2014**, *343*, 66. (h) Sun, L.; Hendon, C. H.; Minier, M. A.; Walsh, A.; Dincă, M. *J. Am. Chem. Soc.* **2015**, *137*, 6164. (i) Park, S. S.; Hontz, E. R.; Sun, L.; Hendon, C. H.; Walsh, A.; Van Voorhis, T.; Dincă, M. *J. Am. Chem. Soc.* **2015**, *137*, 1774.

(6) (a) Hmadeh, M.; Lu, Z.; Liu, Z.; Gándara, F.; Furukawa, H.; Wan, S.; Augustyn, V.; Chang, R.; Liao, L.; Zhou, F.; Perre, E.; Ozolins, V.; Suenaga, K.; Duan, X.; Dunn, B.; Yamamto, Y.; Terasaki, O.; Yaghi, O. M. *Chem. Mater.* **2012**, *24*, 3511. (b) Kambe, T.; Sakamoto, R.; Hoshiko, K.; Takada, K.; Miyachi, M.; Ryu, J.-H.; Sasaki, S.; Kim, J.; Nakazato, K.; Takata, M.; Nishihara, H. *J. Am. Chem. Soc.* **2013**, *135*, 2462. (c) Kambe, T.; Sakamoto, R.; Kusamoto, T.; Pal, T.; Fukui, N.; Hoshiko, K.; Shimojima, T.; Wang, Z.; Hirahara, T.; Ishizaka, K.; Hasegawa, S.; Liu, F.; Nishihara, H. *J. Am. Chem. Soc.* **2014**, *136*, 14357. (d) Sheberla, D.; Sun, L.; Blood-Forsythe, M. A.; Er, S.; Wade, C. R.; Brozek, C. K.; Aspuru-Guzik, A.; Dincă, M. *J. Am. Chem. Soc.* **2014**, *136*, 8859. (e) Campbell, M. G.; Sheberla, D.; Liu, S. F.; Swager, T. M.; Dincă, M. *Angew. Chem., Int. Ed.* **2015**, *54*, 4349. (f) Huang, X.; Sheng, P.; Tu, Z.; Zhang, F.; Wang, J.; Geng, H.; Zou, Y.; Di, C.-A.; Yi, Y.; Sun, Y.; Xu, W.; Zhu, D. *Nat. Commun.* **2015**, *6*, 7408.

(7) Hendon, C. H.; Tiana, D.; Walsh, A. *Phys. Chem. Chem. Phys.* **2012**, *14*, 13120.

(8) (a) Kitagawa, S.; Kawata, S. *Coord. Chem. Rev.* **2002**, *224*, 11. (b) Guo, D.; McCusker, J. K. *Inorg. Chem.* **2007**, *46*, 3257.

(9) (a) Pierpont, C. G.; Francesconi, L. C. *Inorg. Chem.* **1977**, *16*, 2367. (b) Dei, A.; Gatteschi, D.; Pardi, L.; Russo, U. *Inorg. Chem.* **1991**, *30*, 2589. (c) Ward, M. D. *Inorg. Chem.* **1996**, *35*, 1712. (d) Min, K. S.; Rheingold, A. L.; DiPasquale, A.; Miller, J. S. *Inorg. Chem.* **2006**, *45*, 6135. (e) Min, K. S.; DiPasquale, A. G.; Golen, J. A.; Rheingold, A. L.; Miller, J. S. *J. Am. Chem. Soc.* **2007**, *129*, 2360. (f) Min, K. S.; Swierczek, K.; DiPasquale, A. G.; Rheingold, A. L.; Reiff, W. M.; Arif, A. M.; Miller, J. S. *Chem. Commun.* **2008**, 317. (g) Min, K. S.;

DiPasquale, A. G.; Rheingold, A. L.; White, H. S.; Miller, J. S. *J. Am. Chem. Soc.* **2009**, *131*, 6229.

(10) Das, H. S.; Weisser, F.; Schweinfurth, D.; Su, C. Y.; Bogani, L.; Fiedler, J.; Sarkar, B. *Chem. - Eur. J.* **2010**, *16*, 2977.

(11) Abrahams, B. F.; Hudson, T. A.; McCormick, L. J.; Robson, R. *Cryst. Growth Des.* **2011**, *11*, 2717.

(12) Benmansour, S.; Vallés-García, C.; Gómez-Claramunt, P.; Mínguez Espallargas, G.; Gómez-García, C. J. *Inorg. Chem.* **2015**, *54*, 5410.

(13) (a) Luo, T.-T.; Liu, Y.-H.; Tsai, H.-L.; Su, C.-C.; Ueng, C.-H.; Lu, K.-L. *Eur. J. Inorg. Chem.* **2004**, *2004*, 4253. (b) Atzori, M.; Benmansour, S.; Mínguez Espallargas, G.; Clemente-León, M.; Abhervé, A.; Gómez-Claramunt, P.; Coronado, E.; Artizzu, F.; Sessini, E.; Deplano, P.; Serpe, A.; Mercuri, M. L.; Gómez-García, C. J. *Inorg. Chem.* **2013**, *52*, 10031.

(14) (a) Wrobleski, J. T.; Brown, D. B. *Inorg. Chem.* **1979**, *18*, 498. (b) Wrobleski, J. T.; Brown, D. B. *Inorg. Chem.* **1979**, *18*, 2738. (c) Kawata, S.; Kitagawa, S.; Kumagai, H.; Ishiyama, T.; Honda, K.; Tobita, H.; Adachi, K.; Katada, M. *Chem. Mater.* **1998**, *10*, 3902.

(15) (a) Tamaki, H.; Zhong, Z. J.; Matsumoto, N.; Kida, S.; Koikawa, M.; Achiwa, N.; Hashimoto, Y.; Okawa, H. *J. Am. Chem. Soc.* **1992**, *114*, 6974. (b) Decurtins, S.; Schmalle, H. W.; Schneuwly, P.; Ensling, J.; Guetlich, P. *J. Am. Chem. Soc.* **1994**, *116*, 9521. (c) Coronado, E.; Galan-Mascaros, J. R.; Gómez-García, C. J.; Martínez-Ferrero, E.; Almeida, M.; Waerenborgh, J. C. *Eur. J. Inorg. Chem.* **2005**, *2005*, 2064. (d) Clemente-León, M.; Coronado, E.; Gómez-García, C. J.; Soriano-Portillo, A. *Inorg. Chem.* **2006**, *45*, 5653.

(16) Baum, A. E.; Lindeman, S. V.; Fiedler, A. T. *Chem. Commun.* **2013**, *49*, 6531.

(17) Buchanan, R. M.; Kessel, S. L.; Downs, H. H.; Pierpont, C. G.; Hendrickson, D. N. *J. Am. Chem. Soc.* **1978**, *100*, 7894.

(18) (a) Férey, G.; Millange, F.; Morcrette, M.; Serre, C.; Doublet, M.-L.; Grenèche, J.-M.; Tarascon, J.-M. *Angew. Chem., Int. Ed.* **2007**, *46*, 3259. (b) Fateeva, A.; Horcajada, P.; Devic, T.; Serre, C.; Marrot, J.; Grenèche, J.-M.; Morcrette, M.; Tarascon, J.-M.; Maurin, G.; Férey, G. *Eur. J. Inorg. Chem.* **2010**, 3789. (c) Zhang, Z.; Yoshikawa, H.; Awaga, K. *J. Am. Chem. Soc.* **2014**, *136*, 16112. (d) Shin, J.; Kim, M.; Cirera, J.; Chen, S.; Halder, G. J.; Yersak, T. A.; Paesani, F.; Cohen, S. M.; Meng, Y. S. *J. Mater. Chem. A* **2015**, *3*, 4738.

(19) Shaikh, N.; Goswami, S.; Panja, A.; Wang, X.-Y.; Gao, S.; Butcher, R. J.; Banerjee, P. *Inorg. Chem.* **2004**, *43*, 5908.

(20) (a) Demadis, K. D.; Hartshorn, C. M.; Meyer, T. J. *Chem. Rev.* **2001**, *101*, 2655. (b) D'Alessandro, D. M.; Keene, F. R. *Chem. Rev.* **2006**, *106*, 2270. (c) D'Alessandro, D. M.; Keene, F. R. *Chem. Soc. Rev.* **2006**, *35*, 424. (d) Hankache, J.; Wenger, O. S. *Chem. Rev.* **2011**, *111*, 5138.

(21) Meilikhov, M.; Yusenko, K.; Torrisi, A.; Jee, B.; Mellot-Draznieks, C.; Pöppl, A.; Fischer, R. A. *Angew. Chem., Int. Ed.* **2010**, *49*, 6212.

(22) (a) Abrahams, B. F.; Bond, A. M.; Le, T. H.; McCormick, L. J.; Nafady, A.; Robson, R.; Vo, N. *Chem. Commun.* **2012**, *48*, 11422. (b) Kung, C.-W.; Wang, T. C.; Mondloch, J. E.; Fairen-Jimenez, D.; Gardner, D. M.; Bury, W.; Klingsporn, J. M.; Barnes, J. C.; Van Duyne, R.; Stoddart, J. F.; Wasielewski, M. R.; Farha, O. K.; Hupp, J. T. *Chem. Mater.* **2013**, *25*, 5012. (c) Wade, C. R.; Li, M.; Dincă, M. *Angew. Chem., Int. Ed.* **2013**, *52*, 13377. (d) Cozzolino, A. F.; Brozek, C. K.; Palmer, R. D.; Yano, J.; Li, M.; Dincă, M. *J. Am. Chem. Soc.* **2014**, *136*, 3334. (e) Leong, C. F.; Chan, B.; Faust, T. B.; D'Alessandro, D. M. *Chem. Sci.* **2014**, *5*, 4724.

(23) Miller, J. S. *Chem. Soc. Rev.* **2011**, *40*, 3266.

(24) Manriquez, J. M.; Yee, G. T.; McLean, R. S.; Epstein, A. J.; Miller, J. S. *Science* **1991**, *352*, 1415.

(25) Miyazaki, A.; Yamazaki, H.; Aimatsu, M.; Enoki, T.; Watanabe, R.; Ogura, E.; Kuwatani, Y.; Iyoda, M. *Inorg. Chem.* **2007**, *46*, 3353.

(26) Clérac, R.; O'Kane, S.; Cowen, J.; Ouyang, X.; Heintz, R.; Zhao, H.; Bazile, M. J.; Dunbar, K. R. *Chem. Mater.* **2003**, *15*, 1840.

(27) Mathonière, C.; Nuttall, C. J.; Carling, S. G.; Day, P. *Inorg. Chem.* **1996**, *35*, 1201.

(28) Verdaguer, M.; Bleuzen, A.; Marvaud, V.; Vaissermann, J.; Seuleiman, M.; Desplanches, C.; Scuiller, A.; Train, C.; Garde, R.; Gelly, G.; Lomenech, C.; Rosenman, I.; Veillet, P.; Cartier, C.; Villain, F. *Coord. Chem. Rev.* **1999**, *190*, 1023.

(29) Zhu, Z.; Li, H.; Liang, J.; Tao, Z.; Chen, J. *Chem. Commun.* **2015**, *51*, 1446.

(30) Düren, T.; Millange, F.; Férey, G.; Walton, K. S.; Snurr, R. Q. *J. Phys. Chem. C* **2007**, *111*, 15350.

(31) Surface area was calculated using the crystallographic data obtained for **1** (Table S1) and a crystal density that was calculated by excluding the tetrabutylammonium ions in order to mimic the charge-balanced $Fe^{III}_2(dhbq^{2-})_3$ framework ($\rho_{calcd} = 0.644$ mg/m^3).

(32) Coronado, E.; Day, P. *Chem. Rev.* **2004**, *104*, 5419.